

Antiferromagnetism and chiral d-wave superconductivity from an effective $t - J - D$ model for twisted bilayer graphene

Xingyu Gu,^{1,2} Chuan Chen,^{1,2} Jia Ning Leaw,^{1,2} Evan Laksono,^{1,2}
Vitor M. Pereira,^{1,2} Giovanni Vignale,^{2,3,4} and Shaffique Adam^{1,2,3}

¹*Department of Physics, National University of Singapore, 117542, Singapore*

²*Centre for Advanced 2D Materials and Graphene Research Centre,
National University of Singapore, 117546, Singapore*

³*Yale-NUS College, 16 College Avenue West, 138527, Singapore*

⁴*Department of Physics and Astronomy, University of Missouri, 65201, USA*

Starting from the strong-coupling limit of an extended Hubbard model, we develop a spin-fermion theory to study the insulating phase and pairing symmetry of the superconducting phase in twisted bilayer graphene. Assuming that the insulating phase is an anti-ferromagnetic insulator, we show that fluctuations of the anti-ferromagnetic order in the conducting phase can mediate superconducting pairing. Using a self-consistent mean-field analysis, we find that the pairing wave function has a chiral d-wave symmetry. Consistent with this observation, we show explicitly the existence of chiral Majorana edge modes by diagonalizing our proposed Hamiltonian on a finite-sized system. These results establish twisted bilayer graphene as a promising platform to realize topological superconductivity.

Introduction. Correlated insulating phases and unconventional superconductivity have been recently observed in twisted bilayer graphene (tBG) near the magic twist angle $\theta \approx 1.1^\circ$ [1–3]. This is currently leading to an intense surge of interest partly due to the similarity of its phase diagram and that of high- T_c superconductors. Since the experimental discovery, the nature of the insulating phase and pairing mechanism in tBG have been studied by several theoretical proposals, that start from either a weak or strong coupling limit [4–19]. From the weak coupling point of view, the interaction is included perturbatively to the free-electron band structure, calculated from a continuum model [20, 21]. Because of the van-Hove singularity and Fermi surface nesting [5–7, 9], the system exhibits strong particle-hole fluctuations that can lead to an insulating phase and superconductivity upon doping.

On the other hand, the multiple insulating phases observed in the experiment [3] could justify the strong coupling limit as more appropriate for the reference state. Xu and Balents proposed a $SU(4)$ Hubbard model on a triangular lattice motivated by the fact that the density of electrons in tBG peaks at the AA regions [4]. However, it was later shown that to correctly incorporate the moiré symmetries, one needs to include at least two orbitals in the underlying tight-binding Hamiltonian [5–12]. More recently, by taking into account the unusual shape of the Wannier functions, an extended Hubbard model with a “cluster charge interaction” between the electrons (discussed below) was proposed [10, 11], where the Mott insulating phase and reduced Landau level degeneracy at half-filling are explained by an “inter valley coherence” (IVC) (where the monolayer valley degree of freedom is polarized in xy plane), and the chemical potential at the half-filled moiré band is shifted to the Dirac point. The shifting of Fermi level are schematically shown in Fig.

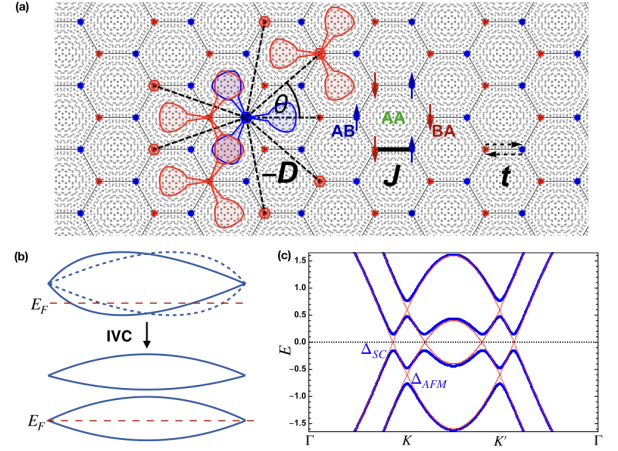


FIG. 1. (a) The underlying moiré pattern and the emergent honeycomb lattice. The lobes show the unusual shape of Wannier functions schematically. The three red Wannier functions share 0, 2 and 1 peaks with the blue Wannier function from top to bottom. The hopping, antiferromagnetic coupling and pairing are denoted as t , J and $-D$, respectively, and the arrows represent the short-range antiferromagnetic order. (b) The occurrence of intervalley coherence order shifts the Fermi level from half-filling to the Dirac point. (c) Gap opening at finite chemical potential. The red line is the non-interacting spectrum and the blue line is the spectrum with non-zero AFM and superconducting gap. The SC gap is at Fermi level (indicated by the dashed line) while AFM gap is at Dirac point. The k path is along the $\Gamma - K - K' - \Gamma$ line in the moiré Brillouin zone.

1(b). This loss of monolayer valley quantum number explains why the experimentally observed Landau level degeneracy close to half filling is half that at charge neutrality. This breaking of valley symmetry (as opposed to spin symmetry) is supported by Hartree-Fock calculations [10], and because experiments suggests spin-singlet

Mott-like behaviour [1], which would require unpolarized spins. The IVC state would still be semi-metallic and, to obtain an insulating phase, further symmetry breaking must take place to gap the Dirac cone.

Reference [16] explored the possible symmetry-broken phases using quantum Monte Carlo calculations for such a cluster charge interaction and, as in monolayer graphene when the contact interaction dominates over the long-range Coulomb interaction, the ground state in the strong coupling limit has anti-ferromagnetic (AFM) order [22]. Although the AFM insulating phase in this model has the same origin as in the monolayer, the cluster charge interaction reduces the effective on-site repulsion, and this might explain the small gap of the insulating phase observed experimentally. Unlike monolayer graphene, the Monte Carlo results also found a Kekulé valence bond solid phase at intermediate coupling, but this is not germane to our considerations here.

In this Letter, we start from the above-mentioned strong coupling AFM limit with assumed intervalley coherence order. Due to the valley $U(1)$ symmetry breaking, there is no topological obstruction to build up a tight binding model [17]. We show that the low energy physics is governed by a $t - J - D$ model, $H = H_t + H_J + H_D$, where

$$H_t = -t \sum_{\langle ij \rangle, \alpha} a_{i\alpha}^\dagger b_{j\alpha} + h.c. \quad (1a)$$

$$H_J = J \sum_{\langle ij \rangle} \vec{S}_i \cdot \vec{S}_j \quad (1b)$$

$$H_D = -D \sum_{\langle\langle ij \rangle\rangle} h_{ij}^\dagger h_{ij} \quad (1c)$$

Here, t is hopping parameter, i, j are sites of the honeycomb lattice defined by the AB, BA regions in the moiré lattice, a and b are the electron operators corresponding to two sublattices, α indicates spin, $\langle\langle ij \rangle\rangle$ in Eq. (1c) represents the blue and red pairs in Fig. 1a. D is the pairing strength, $h_{ij} = a_{i\uparrow}^\dagger b_{j\downarrow} - a_{i\downarrow}^\dagger b_{j\uparrow}$ is the inter-sublattice singlet operator. J is AFM coupling and \vec{S} is the spin operator. Note that, unlike in the approach to cuprates or pnictides [23], in this model the superconducting pairing couples not the nearest but remote neighbors, as schematically shown in Fig. 1(a).

Based on this Hamiltonian, our main conclusion is that the pairing symmetry in tBG should be chiral $d+id$ (this is consistent with findings using other models used for tBG, including Refs.[4, 6, 13, 14, 18, 19]). The advantage of our explicit Hamiltonian is that we can directly demonstrate that quantum fluctuations of the AFM order mediate an attractive pairing interaction. Moreover, since we have the form of that pairing in real space, using a finite size geometry, we can prove the existence of chiral Majorana modes that should be observable in experiments.

Effective model. To derive Eq. (1), we start from the following real-space Hamiltonian $H = H_t + H_U$ on a honeycomb lattice [10, 11], where

$$H_t = -t \sum_{\langle ij \rangle, \alpha} a_{i\alpha}^\dagger b_{j\alpha} + h.c. \quad (2a)$$

$$H_U = U \sum_R (Q_R - 2)^2 \quad (2b)$$

Here R marks the position of each hexagon's center, and $Q_R = \sum_{i \in \square} \sum_\alpha \frac{n_{i\alpha}}{3}$ is the charge located at that position.

Compared to the onsite Hubbard interaction, there is repulsive Coulomb interaction between electrons sharing the hexagon in this model. This unusual form of interaction originates from the extended nature of the Wannier functions in tBG. For the flat bands in tBG, it is known that the associated electron density peaks form a triangular lattice [1]. In contrast, symmetry dictates that the Wannier centers span a honeycomb lattice [8, 10–12]. The system accommodates these constraints by exhibiting Wannier functions with a three-lobed shape [11, 12]. While these are centered at the honeycomb sites, the spatial superposition of the Wannier functions at the corners of a hexagon creates maxima of the electronic density at its center. As a result, there is overlap of 3, 2, 1 peak(s) when considering the interaction between on-site, NN, next NN (NNN) and third NN electrons. This determines the interaction strength ratio from onsite to third NN to be 3:2:1:1. The Wannier functions are schematically shown in Fig. 1(a).

Since the interaction is larger on-site than among NN, an anti-ferromagnetic coupling $J \sim t^2/U$ arises to leading order in perturbation theory [24] (explaining the numerical discovery of the AFM order in the quantum Monte Carlo [16]). We note in passing that this AFM insulating phase is also consistent with the experimentally observed quantum oscillation data [1–3] as follows: In the IVC theory, considering the spin and moiré valley degree of freedom, the Fermi surface should be four-fold degenerate around half filling, but it is observed only 2-fold degenerate in experiment. This reduction can be understood as the splitting of Landau levels, as has been discussed previously [25–28]. This argument also explains the anomalous FS degeneracy reduction around charge neutrality, compared to bilayer graphene with a larger twist angle $\theta = 1.8^\circ$ [29].

In cuprates and iron pnictides, the AFM coupling is closely related to superconductivity [23], which can be understood using the Fierz identity: $\vec{S}_i \cdot \vec{S}_j = -2h_{ij}^\dagger h_{ij} + n_i n_j$, where h_{ij} is the singlet pairing operator defined above. But in tBG, one expects the NN pairing to be strongly suppressed due to the strong repulsion between electrons in the same hexagon, similarly to how the on-site pairing is suppressed in cuprates and pnictides. Therefore, to determine the nature and feasibility

TABLE I. Order parameter form

Pairing symmetry	s	$d_{x^2-y^2}$	d_{xy}	$d_{x^2-y^2} + id_{xy}$
form of $f(\theta)$	1	$\cos(2\theta)$	$\sin(2\theta)$	$e^{i2\theta}$

of a superconducting ground state, to leading order we need only consider the pairing between electrons which not sharing a common hexagon, because only these are weakly repelled from each other. In our study, we consider the six nearest ones indicated by the red points in Fig. 1a and we show that such long range pairing can be mediated by the AFM fluctuations. First we sketch the basic physics of AFM mediated SC, a more concrete derivation is shown in supplementary S1. The coupling between AFM order parameter $m_i = \frac{\langle S_a^z \rangle - \langle S_b^z \rangle}{2}$ and the fermions is:

$$H_i = \lambda m_i \sigma_{\alpha\beta}^z (a_{i\alpha}^\dagger a_{i\beta} - b_{i\alpha}^\dagger b_{i\beta}), \quad (3)$$

where λ is the coupling strength. a and b are the electron annihilation operators of the two sublattices. The local magnetization is assumed to be aligned in the z -direction. Here we assume there is no long range AFM order, only the fluctuation is important. The inter-sublattice effective electron-electron interaction can be obtained by integrating out the spin fluctuations, and reads

$$H_{ij} = \lambda^2 \chi_{i,j} \sigma_{\alpha\beta}^z \sigma_{\gamma\delta}^z a_{i\alpha}^\dagger a_{i\beta} b_{j\gamma}^\dagger b_{j\delta}, \quad (4)$$

It arises in an approximation that neglects retardation effects, where χ_{ij} is the static spin susceptibility $\chi_{ij} \propto \frac{1}{g} e^{-R_{ij}/\xi}$, with R_{ij} the distance between unit cells i and j , ξ the magnetic correlation length, and g the spin stiffness (see supplementary information for details). It is easy to see that H_{ij} is attractive for anti-parallel spins, in which case $\alpha = \beta = -\gamma = -\delta$. The attractive interaction $D \sim \frac{\lambda^2}{g} e^{-R_{ij}/\xi}$ is significant as long as spin fluctuation are strong (ξ is large) even though the AFM order itself doesn't develop. This attractive interaction between anti-parallel spins leads to singlet superconductivity [30], which will be our focus here since it was furthermore suggested by the experimental results [2].

Moreover, using similar arguments, one finds that the intra-sublattice interaction between anti-parallel spin is repulsive. Such a staggered “attractive-repulsive-attractive” profile is similar to cuprates, where it arises from Fermi surface nesting [30–32]. This similarity between pairing mechanism provides some unification between tBG and cuprates. In this work, for simplicity, we only consider the nearest pairing possibilities. In the following, we study the ground state of the Hamiltonian in Eq.(1) consisting of the kinetic energy, anti-ferromagnetic coupling between NN sites and a singlet pairing term.

Pairing symmetry. Before studying the interplay between AFM and SC phases, we tackle the SC instability

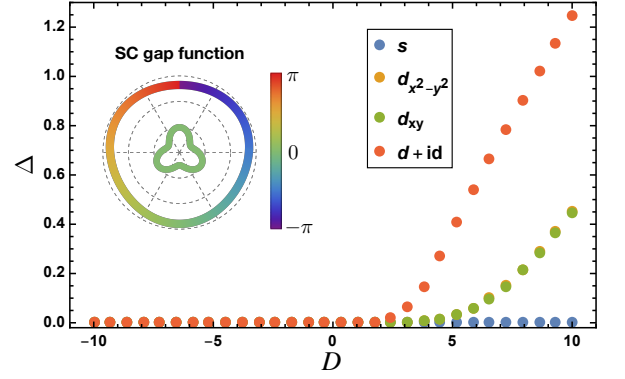


FIG. 2. Solution of gap equation (6) for different pairing symmetries. The s -wave order parameter is always very small, while the latter three pairing symmetries develop finite order parameter at finite D . The solution for $d_{x^2-y^2}$ in and d_{xy} are exactly degenerate, which is protected by symmetry. The D_c of $d + id$ is the smallest, indicating it to be the ground state. The inset shows the magnitude and phase of the s - and $d + id$ -wave gap functions along a circle centered at the Dirac point with radius $0.1/a$ when real space order parameter Δ is fixed to be 1. The radius of the ring shows magnitude and the color shows phase. The outer ring represents $d + id$ and the inner ring represents s -wave. For clarity, the magnitude of the s -wave order parameter has been increased by a factor of five.

first (with $J = 0$) and fix the pairing symmetry. The order parameter in real space is defined as $\Delta_{ij} = D \langle h_{ij} \rangle$. The mean field interaction reads

$$H_D^{MF} = \sum_{i,\mathbf{a}} -\Delta_{i,\mathbf{a}} h_{i,i+\mathbf{a}}^\dagger - \Delta_{i,\mathbf{a}}^* h_{i,i+\mathbf{a}} + \frac{6N}{D} |\Delta|^2 \\ \cong - \sum_{\mathbf{k}} D_{\mathbf{k}} c_{\mathbf{k}\uparrow}^\dagger c_{-\mathbf{k}\downarrow}^\dagger + h.c. + \frac{6N}{D} |\Delta|^2, \quad (5)$$

where the $\Delta_{i,\mathbf{a}} = \Delta_{i,i+\mathbf{a}}$ denotes the pairing between site i and $i + \mathbf{a}$, with \mathbf{a} representing the six vectors connecting the blue and the red sites. In the second line, c is the conduction fermion annihilation operator, $D_{\mathbf{k}} = \sum_{\mathbf{a}} \Delta_{\mathbf{a}} \cos(\mathbf{k} \cdot \mathbf{a} - \phi_{\mathbf{k}})$ is the SC gap. In the expression of $D_{\mathbf{k}}$, $\Delta_{\mathbf{a}}$ are the SC order parameters defined on the six bonds and $\phi_{\mathbf{k}} = \arg(\sum_{\delta} e^{i\mathbf{k} \cdot \delta})$, where δ are the three vectors connecting the NN sites. To get this result, we have replaced the electron operators in the sublattice representation by electron operators in the band representation and keep only the intra-conduction band pairing term, since it is the most important term at finite chemical potential where SC is observed experimentally (The detailed derivation of the mean field Hamiltonian Eq.(5) is shown in supplementary section S-II).

We consider the four different pairing symmetries indicated in Table. I: s -wave, $d_{x^2-y^2}$ -wave, d_{xy} -wave and $d_{x^2-y^2} + id_{xy}$ -wave. They are defined by $\Delta_{\mathbf{a}} = \Delta f(\theta_{\mathbf{a}})$, with $\theta_{\mathbf{a}}$ the angle between the bonds and the $+x$ -axis, as shown in Fig. 1a.

The pairing symmetry in the ground state has been obtained by a self-consistent mean field analysis. The spectrum of the Bogoliubov-de Gennes (BdG) Hamiltonian is (See supplementary section S-IV for more details): $E_{\mathbf{k}} = \pm \sqrt{(\epsilon_{\mathbf{k}} - \mu)^2 + |D_{\mathbf{k}}|^2}$ and $\epsilon_{\mathbf{k}} = t\sqrt{3 + 2\cos(\sqrt{3}k_y) + 4\cos(\frac{\sqrt{3}k_y}{2})\cos(\frac{3k_x}{2})}$ is the energy dispersion of free electrons in the honeycomb lattice [33]. By minimizing the free energy, we obtain the gap equation:

$$\sum_{\mathbf{k}} \frac{1}{N} \frac{|\sum_{\mathbf{a}} f(\theta_{\mathbf{a}})|^2}{E_{\mathbf{k}}} = \frac{12}{D}, \quad (6)$$

where N is the number of unit cells. The solutions of this gap equation as a function of D for different pairing symmetries are shown in Fig. 2. We choose $\mu = 0.2$ for illustration and use the hopping t as the unit of energy. For repulsive interaction ($D < 0$), there is obviously no superconductivity at all. For attractive interactions ($D > 0$), while the s-wave order parameter remains zero for D up to 10, a nonzero d-wave order parameter emerges at a finite critical interaction D_c . The two different d-wave phases are exactly degenerate, which is protected by symmetry. The case $d + id$ has both the smallest D_c and larger order parameter magnitude at given D . This implies the ground state should be $d + id$. In tBG, due to the small bandwidth, t is extremely small [11] and the attractive interaction strength can exceed D_c easily. We note that a similar $d + id$ SC phase is obtained in monolayer graphene [34], if one considers only NN pairing. Hence, $d + id$ pairing is likely a robust feature of correlation-driven SC in honeycomb lattices in the strong coupling limit. But, crucially, whereas in monolayer graphene the interaction strength is too weak ($\frac{U}{t} \sim 3.3$ [35, 36]) while, in tBG, the flat band drives the system into strong coupling ($\frac{U}{t} \sim 50$ [11]), making it an ideal platform to realize topological superconductivity.

In order to understand the favouring of $d + id$ pairing symmetry, we study the different gap functions in momentum space with the real-space amplitudes $\Delta_{i,\mathbf{a}}$ fixed to be unit and compare the behavior of $D_{\mathbf{k}}$. Since the reduction of free energy is dominated by the gap opening at the Fermi surface, we plot the SC gap along the circle centered at the Dirac point with radius $0.1/a$, where a is the lattice constant of the emergent honeycomb lattice. The cases of s-wave and $d + id$ are shown in the inset of Fig. 2. The gap due to the former is significantly smaller than that arising from d-wave pairing, which means d-wave is more favourable in energy. We notice that the same argument have also been used to determine the pairing symmetry in cuprates and iron pnictides [23]. This provides another opportunity to unify tBG and high- T_c superconductors. In addition, we find that while the s-wave order parameter has a trivial phase (given by the color scale in the inset of Fig. 2), the $d + id$ case displays a nontrivial winding phase of 2π , making it qualitatively similar to

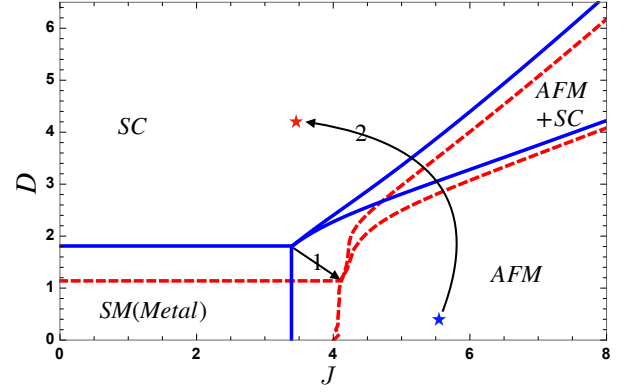


FIG. 3. Mean field phase diagram for $\mu = 0$ (blue solid line) and $\mu = 0.3$ (red dashed line). The system is (semi-)metallic in the weak coupling region. In the strong J limit, it becomes AFM ordered and in the strong D limit, it is superconducting. Arrow 1 shows qualitatively the increase in J_c and decrease in D_c upon doping, while arrow 2 shows the transition from AFM state to SC observed experimentally when tuning chemical potential.

the case of $p + ip$ symmetry in monolayer graphene. [37].

Interplay between AFM and SC. We now reinstate the AFM interaction ($J \neq 0$) and probe the relative stability of the two phases according to the full Hamiltonian in Eq. (1). According to the discussion above, we consider here a $d + id$ superconducting pairing symmetry. The spectrum of the BdG Hamiltonian is: $E_{\mathbf{k}} = \pm \sqrt{\epsilon_{\mathbf{k}}^2 + m^2 + \mu^2 + |D_{\mathbf{k}}|^2} \pm 2\sqrt{(\epsilon_{\mathbf{k}}^2 + m^2)\mu^2}$, where m is the AFM order parameter as defined in Eq. 3. The coupled gap equations are:

$$\frac{6}{J} = \sum_{l=\pm 1} \frac{1}{N_{\mathbf{k}}} \frac{1 + l \frac{\mu^2}{\sqrt{(\epsilon_{\mathbf{k}}^2 + m^2)\mu^2}}}{\sqrt{(\epsilon_{\mathbf{k}}^2 + m^2 + \mu^2 + |D_{\mathbf{k}}|^2 + 2l\sqrt{(\epsilon_{\mathbf{k}}^2 + m^2)\mu^2})}} \quad (7a)$$

$$\frac{12}{D} = \sum_{l=\pm 1} \frac{1}{N_{\mathbf{k}}} \frac{|\sum_{\mathbf{a}} f_{\mathbf{a}}|^2}{\sqrt{(\epsilon_{\mathbf{k}}^2 + m^2 + \mu^2 + |D_{\mathbf{k}}|^2 + 2l\sqrt{(\epsilon_{\mathbf{k}}^2 + m^2)\mu^2})}} \quad (7b)$$

where $N_{\mathbf{k}}$ is the number of \mathbf{k} points in the summation. Here, we use $l = +/ - 1$ to distinguish the valence/conduction bands in the original Dirac dispersion. In the $m = 0$ limit, if we only consider the $l = -1$ part of Eq. 7b, it reduces to Eq. 6. The appearance of the $l = 1$ is because here we consider intra-valence band pairing. At finite chemical potential (which is the regime where SC emerges), the $l = 1$ term always has a larger denominator and is therefore less important.

Figure 3 shows the mean field phase diagram. The blue solid line is for $\mu = 0$ while the red dashed line is for $\mu = 0.3$. In both cases, the system is (semi-)metallic in the weak-coupling region. In the strong J limit, it is

AFM ordered while in the strong D limit, it is superconducting, as expected. The opposite trend (indicated by arrow 1 in Fig. 3) of D_c (which decreases) and J_c (which increases) with doping implies that the competition between the two orders favours SC at higher carrier densities, and can be understood as follows: AFM order opens a gap at the Dirac point. Upon doping, the energy gain of AFM state becomes smaller, which means a larger critical interaction is required. On the other hand, SC opens a gap at Fermi surface, a larger Fermi surface at finite doping indicates a smaller D_c . The gaps opening by AFM and SC order are shown in Fig. 1(c). This behavior is consistent with the effect of doping seen experimentally where doping drives tBG from an insulating to a SC state at low temperature: At half-filling, the tBG is insulating [1], which our model indicates should correspond to an AFM insulating ground state. Starting from the AFM phase at $\mu = 0$ in the diagram of Fig. 3, our results show that its stability is progressively reduced by adding more carriers, and ultimately replaced by a SC ground state beyond a critical doping. Note that the AFM-SC transition is not simply a consequence of the doping dependence of J_c and D_c . In addition to that, $\frac{J}{t}$ is expected to decrease with doping [38] and enhance magnetic fluctuations. These, in turn, increase V according to Eq. 4 further facilitating that phase transition. The transition from AFM insulating state to SC state is indicated by arrow 2 in Fig. 3.

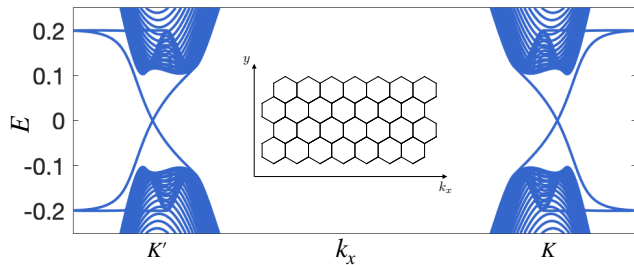


FIG. 4. tBG supports chiral Majorana modes in cylinder geometry. There is one chiral Majorana mode for each valley, which is due to the $p+ip$ pairing around each Dirac point. The inset shows the geometry we use. We take periodic boundary condition and open boundary condition in y direction.

Chiral Majorana modes. It is known that the topology of the chiral $d+id$ pairing is non-trivial because its Chern number is 2. As a result, there should be chiral Majorana modes localized at the edge in a finite size system. To show explicitly the existence of chiral Majorana modes, we studied a finite (one direction) system with a cylinder geometry as can be seen in the inset of Fig. 4. We take a periodic boundary condition along the x direction and an open boundary condition along the y direction. By diagonalizing the finite size Hamiltonian, we obtain the spectrum in Fig. 4. For each Dirac cone, there is one chiral edge mode at each edge. This result is consistent

with the observation that the pairing has a $p+ip$ feature around each Dirac cone. Near each edge, there are two chiral edge states in total, reflecting the $C = 2$ nature of the $d+id$ pairing. The existence of these chiral Majorana modes can be detected in transport experiment [39].

Acknowledgements. We thank Nimisha Raghuvanshi for helpful discussions. This work is supported by the Singapore Ministry of Education MOE2017-T2-1-130 and MOE2017-T2-2-140.

-
- [1] Yuan Cao, Valla Fatemi, Ahmet Demir, Shiang Fang, Spencer L Tomarken, Jason Y Luo, Javier D Sanchez-Yamagishi, Kenji Watanabe, Takashi Taniguchi, Efthimios Kaxiras, et al. Correlated insulator behaviour at half-filling in magic-angle graphene superlattices. *Nature*, 556(7699):80, 2018.
 - [2] Yuan Cao, Valla Fatemi, Shiang Fang, Kenji Watanabe, Takashi Taniguchi, Efthimios Kaxiras, and Pablo Jarillo-Herrero. Unconventional superconductivity in magic-angle graphene superlattices. *Nature*, 556(7699):43, 2018.
 - [3] Matthew Yankowitz, Shaowen Chen, Hryhorii Polshyn, Yuxuan Zhang, K Watanabe, T Taniguchi, David Graf, Andrea F Young, and Cory R Dean. Tuning superconductivity in twisted bilayer graphene. *Science*, page eaav1910, 2019.
 - [4] Cenke Xu and Leon Balents. Topological superconductivity in twisted multilayer graphene. *Phys. Rev. Lett.*, 121:087001, Aug 2018.
 - [5] Hiroki Isobe, Noah F. Q. Yuan, and Liang Fu. Unconventional superconductivity and density waves in twisted bilayer graphene. *Phys. Rev. X*, 8:041041, Dec 2018.
 - [6] Cheng-Cheng Liu, Li-Da Zhang, Wei-Qiang Chen, and Fan Yang. Chiral spin density wave and $d+id$ superconductivity in the magic-angle-twisted bilayer graphene. *Phys. Rev. Lett.*, 121:217001, Nov 2018.
 - [7] Evan Laksono, Jia Ning Leaw, Alexander Reaves, Manraaj Singh, Xinyun Wang, Shaffique Adam, and Xingyu Gu. Singlet superconductivity enhanced by charge order in nested twisted bilayer graphene fermi surfaces. *Solid State Communications*, 282:38–44, 2018.
 - [8] Noah F. Q. Yuan and Liang Fu. Model for the metal-insulator transition in graphene superlattices and beyond. *Phys. Rev. B*, 98:045103, Jul 2018.
 - [9] Yi-Zhuang You and Ashvin Vishwanath. Superconductivity from valley fluctuations and approximate $so(4)$ symmetry in a weak coupling theory of twisted bilayer graphene. *arXiv preprint arXiv:1805.06867*, 2018.
 - [10] Hoi Chun Po, Liujun Zou, Ashvin Vishwanath, and T. Senthil. Origin of mott insulating behavior and superconductivity in twisted bilayer graphene. *Phys. Rev. X*, 8:031089, Sep 2018.
 - [11] Mikito Koshino, Noah FQ Yuan, Takashi Koretsune, Masayuki Ochi, Kazuhiko Kuroki, and Liang Fu. Maximally localized wannier orbitals and the extended hubbard model for twisted bilayer graphene. *Physical Review X*, 8(3):031087, 2018.
 - [12] Jian Kang and Oskar Vafeek. Symmetry, maximally localized wannier states, and a low-energy model for twisted bilayer graphene narrow bands. *Phys. Rev. X*, 8:031088,

- Sep 2018.
- [13] Huaiming Guo, Xingchuan Zhu, Shiping Feng, and Richard T. Scalettar. Pairing symmetry of interacting fermions on a twisted bilayer graphene superlattice. *Phys. Rev. B*, 97:235453, Jun 2018.
 - [14] Tongyun Huang, Lufeng Zhang, and Tianxing Ma. Antiferromagnetically ordered mott insulator and $d + id$ superconductivity in twisted bilayer graphene: A quantum monte carlo study. *arXiv preprint arXiv:1804.06096*, 2018.
 - [15] J. F. Dodaro, S. A. Kivelson, Y. Schattner, X. Q. Sun, and C. Wang. Phases of a phenomenological model of twisted bilayer graphene. *Phys. Rev. B*, 98:075154, Aug 2018.
 - [16] Xiao Yan Xu, K. T. Law, and Patrick A. Lee. Kekulé valence bond order in an extended hubbard model on the honeycomb lattice with possible applications to twisted bilayer graphene. *Phys. Rev. B*, 98:121406, Sep 2018.
 - [17] Liujun Zou, Hoi Chun Po, Ashvin Vishwanath, and T. Senthil. Band structure of twisted bilayer graphene: Emergent symmetries, commensurate approximants, and wannier obstructions. *Phys. Rev. B*, 98:085435, Aug 2018.
 - [18] Maciej Fidrysiak, M Zegrodnik, and Józef Spałek. Unconventional topological superconductivity and phase diagram for an effective two-orbital model as applied to twisted bilayer graphene. *Physical Review B*, 98(8):085436, 2018.
 - [19] Xiao-Chuan Wu, Chao-Ming Jian, and Cenke Xu. Coupled wire description of the correlated physics in twisted bilayer graphene. *arXiv preprint arXiv:1811.08442*, 2018.
 - [20] Rafi Bistritzer and Allan H MacDonald. Moiré bands in twisted double-layer graphene. *Proceedings of the National Academy of Sciences*, 108(30):12233–12237, 2011.
 - [21] JMB Lopes Dos Santos, NMR Peres, and AH Castro Neto. Graphene bilayer with a twist: Electronic structure. *Physical review letters*, 99(25):256802, 2007.
 - [22] Ho-Kin Tang, JN Leaw, JNB Rodrigues, IF Herbut, P Sengupta, FF Assaad, and S Adam. The role of electron-electron interactions in two-dimensional dirac fermions. *Science*, 361(6402):570–574, 2018.
 - [23] Jiangping Hu. Identifying the genes of unconventional high temperature superconductors. *Science bulletin*, 61(7):561–569, 2016.
 - [24] PW Anderson. Antiferromagnetism. theory of superexchange interaction. *Physical Review*, 79(2):350, 1950.
 - [25] Min-Young Choi, Young-Hwan Hyun, and Yoonbai Kim. Angle dependence of the landau level spectrum in twisted bilayer graphene. *Physical review B*, 84(19):195437, 2011.
 - [26] R De Gail, MO Goerbig, F Guinea, G Montambaux, and AH Castro Neto. Topologically protected zero modes in twisted bilayer graphene. *Physical Review B*, 84(4):045436, 2011.
 - [27] Dong Su Lee, Christian Riedl, Thomas Beringer, AH Castro Neto, Klaus von Klitzing, Ulrich Starke, and Jurgen H Smet. Quantum hall effect in twisted bilayer graphene. *Physical review letters*, 107(21):216602, 2011.
 - [28] Pilkyung Moon and Mikito Koshino. Energy spectrum and quantum hall effect in twisted bilayer graphene. *Physical Review B*, 85(19):195458, 2012.
 - [29] Y Cao, JY Luo, V Fatemi, S Fang, JD Sanchez-Yamagishi, K Watanabe, T Taniguchi, E Kaxiras, and P Jarillo-Herrero. Superlattice-induced insulating states and valley-protected orbits in twisted bilayer graphene. *Physical review letters*, 117(11):116804, 2016.
 - [30] D. J. Scalapino, E. Loh, and J. E. Hirsch. Fermi-surface instabilities and superconducting d-wave pairing. *Phys. Rev. B*, 35:6694–6698, May 1987.
 - [31] G. Vignale and K. S. Singwi. Superconducting pairing of holes in the antiferromagnetic state of the two-dimensional hubbard model. *Phys. Rev. B*, 39:2956–2959, Feb 1989.
 - [32] G. Vignale and M. R. Hedayati. Motion of a single hole in an itinerant-electron antiferromagnet. *Phys. Rev. B*, 42:786–797, Jul 1990.
 - [33] AH Castro Neto, Francisco Guinea, Nuno MR Peres, Kostya S Novoselov, and Andre K Geim. The electronic properties of graphene. *Reviews of modern physics*, 81(1):109, 2009.
 - [34] Annica M Black-Schaffer and Carsten Honerkamp. Chiral d-wave superconductivity in doped graphene. *Journal of Physics: Condensed Matter*, 26(42):423201, 2014.
 - [35] TO Wehling, E Şaşıoğlu, C Friedrich, AI Lichtenstein, MI Katsnelson, and S Blügel. Strength of effective coulomb interactions in graphene and graphite. *Physical review letters*, 106(23):236805, 2011.
 - [36] Ho-Kin Tang, E Laksono, JNB Rodrigues, Pinaki Sengupta, FF Assaad, and S Adam. Interaction-driven metal-insulator transition in strained graphene. *Physical review letters*, 115(18):186602, 2015.
 - [37] A. M. Black-Schaffer and K. Le Hur. Topological superconductivity in two dimensions with mixed chirality. *Phys. Rev. B*, 92:140503, Oct 2015.
 - [38] Fu-Chen Zhang, Claudius Gros, T Maurice Rice, and Hiroyuki Shiba. A renormalised hamiltonian approach to a resonant valence bond wavefunction. *Superconductor Science and Technology*, 1(1):36, 1988.
 - [39] Qing Lin He, Lei Pan, Alexander L Stern, Edward C Burks, Xiaoyu Che, Gen Yin, Jing Wang, Biao Lian, Quan Zhou, Eun Sang Choi, et al. Chiral majorana fermion modes in a quantum anomalous hall insulator–superconductor structure. *Science*, 357(6348):294–299, 2017.